Numerical Simulation of the Evolution of Stress in Solar Cells During the Entire Manufacturing Cycle of a Conventional Silicon Wafer Based Photovoltaic Laminate

W. J. R. Song, Sasi Kumar Tippabhotla, A. A. O. Tay, and A. S. Budiman

***Abstract*—A significant amount of failure and fracture in solar cells have been observed during the soldering and lamination of a photovoltaic (PV) module. This implies that high residual stresses are developed in the cells. In this paper, the evolution of stresses in solar cells throughout the manufacturing cycle of a conventional PV laminate is simulated in a sequential step-by-step manner such that the residual stresses at the end of one step is brought forward to the next. By analyzing the principal stresses generated in the cells, the critical instances in the manufacturing cycle can be identified. The accumulated final residual stresses in the PV laminate are determined, which include the postsoldering, lamination, and post-lamination thermal stresses because of the coefficient of thermal expansion mismatch between the laminate constituent materials. In addition, stresses in the cells during the pressure-ramping step of the lamination process are determined and found to be the most critical in the entire PV laminate manufacturing cycle. The effect of cell thickness on the evolution of stresses in the cells throughout the manufacturing cycle of a conventional PV laminate are also investigated.**

***Index Terms*—Crystalline silicon cell, encapsulation, lamination stress, soldering stress, thermomechanical (TM) residual stress.**

I. Introduction

CRACKS in silicon wafer solar cells is a major concern in the photovoltaics (PV) industry. Because of the way they are manufactured, silicon (Si) wafer solar cells often contain microcracks that may grow into larger cracks during their integration into a PV module [1]. These cracks could be further propagated by external loads during the transportation and installation of the modules. Crack propagation could also occur during field operation when the modules are subjected to wind loads, snow loads, and temperature cycling. The implications of large cell cracks are tremendous as they represent module failure and replacement costs to the manufacturer. Even if the propagation of cracks does not result in catastrophic fracture of cells, they will give rise to significant power loss over time. The existence of cracks in PV modules is often detected using electroluminescence (EL) where a current is transmitted through the cells in a module and areas of the cells that have cracks are revealed as dark patches. A typical EL image is shown in Fig. 1 where it can be seen that almost all the cracks in the solar cells are located adjacent to the edges of the interconnects.

Fig. 1. Typical EL image of a PV module showing that the majority of cracks (dark regions) in silicon cells occur along the edges of the interconnects [2].

It is now widely known that the effects of cracking in Si cells in PV modules have an adverse effect on the output power. Coupled with residual thermal stresses and mechanical loads during field operation, these cracks may propagate and create electrical separation and nonoperational parts of the cell as observed by the dark patches during EL testing [2]. Kajari-Schroeder *et al.* [3] have also carried out EL studies on the distribution of cell cracks in PV modules subjected to the IEC61215 mechanical load test where they found that 50% of the crack orientation in cells were parallel to the copper interconnects and the cells with the highest number of cracks were located near the corners of the PV module.

In an experimental study of mechanical characterization in PV modules, Sander *et al.* [4] employed methods such as laser doppler vibrometry and digital image correlation to measure the postlamination warpage of PV laminates. However, these methods only measured the deformations of the PV laminates

Manuscript received May 28, 2017; revised September 12, 2017 and October 18, 2017; accepted November 1, 2017. Date of publication December 13, 2017; date of current version December 20, 2017. This work was supported in part by the National Research Foundation (NRF)/Economic Development Board (EDB) of Singapore under the EIRP Grant "(NRF2013EWT–EIRP002–017)—Enabling thin silicon technologies for next generation, lower cost solar PV systems." *(Corresponding author: Arief Suriadi Budiman.)*

The authors are with the Xtreme Photovoltaics Laboratory, Singapore University of Technology and Design, Singapore 487372 (e-mail: ridhuan_song@mymail.sutd.edu.sg; sasi_kumar@mymail.sutd.edu.sg; andrew_tay@sutd.edu.sg; suriadi@alumni.stanford.edu).

Color versions of one or more of the figures in this paper are available online at http://ieeexplore.ieee.org.

Digital Object Identifier 10.1109/JPHOTOV.2017.2775158

and not the stresses in the assembly. Tippabhotla *et al.* [5] took a step further by using synchrotron X-ray submicron diffraction to analyze the residual mechanical stresses in encapsulated monocrystalline Si solar cells after lamination. It was observed that there was a significant increase of residual stress in the Si cell near the solder joints, which explains the phenomenon of silicon cells cracking near soldered interconnects.

Many numerical studies and finite element analysis (FEA) have been carried out to investigate the stresses developed in Si cells because of mismatch in the coefficient of thermal expansion (CTE) of the constituent materials. Kraemer *et al.* [6] analyzed the thermomechanical (TM) stresses developed in the cells after the interconnect soldering process. In their study, three-dimensional (3-D) FE models of two adjacent quarter cells were interconnected by copper interconnects and stresses were induced when the solder solidifies and cools down to room temperature. They found that the largest stress gradients in the cells occurred along the edges of interconnects. However, they did not proceed further to compute the stresses developed after the lamination process.

On the other hand, there have been several studies that computed the postlamination TM stresses in PV modules without incorporating the postsoldering stresses. All such studies assume that the initial stress in the laminate is zero at the lamination temperature. In numerical studies by Dietrich *et al.* [7] and Eitner *et al.* [8], TM stresses in solar cells in PV modules were quantified. Viscoelastic effects of the ethylene vinyl-acetate (EVA) encapsulant were incorporated into the FE simulations and the obtained gap deformation between cells correlated well with those of their experimental results [9], [10].

Lee and Tay [11] performed 3-D FE simulations of a full-sized 72-cell PV laminate to obtain the postlamination TM stresses. They then simulated the stress redistributions within the laminate when it is framed, installed, and subsequently exposed to 1000 $\mathrm{W/m^2}$ of direct sunshine. They investigated the differences in induced TM stresses when using tempered glass covers versus float glass covers. They found that the largest maximum principal stresses in both types of glass covers occur near the corners of the modules. They also found that the largest peeling stresses occur at the edges of the cell-EVA interfaces that indicate the locations where delaminations are likely to initiate [12]. Zhang *et al.* [13] also performed similar simulations of postlamination stress in the PV laminate but they went further to use the submodeling technique to include the soldered copper interconnects in their analysis. However, this does not fully account for the actual postsoldering stress in the laminate since they had assumed that the initial stress in the entire laminate was zero at the lamination temperature, whereas in reality, there is some initial residual stress in the cell–interconnect assembly where the bond was formed at 210 °C. Their results show that the location of maximum stresses experienced in the cell was adjacent to the copper interconnects.

The residual stress in a PV laminate is the result of the accumulation of residual stresses from each segment of the manufacturing cycle. In an attempt to obtain the accumulated stresses in the cells, Dietrich *et al.* [14] approximated the lamination process to flatten the cell between two rigid surfaces. They obtained the stresses in the cell because of the flattening using FEA and then exported the cell stresses to a second FE model from which they simulated the postlamination cooldown process. They then used linear superposition with the postsoldering stresses from a separate FEA to obtain the accumulated cell stresses in the laminate. While the above is an attempt to obtain the accumulated stresses in the laminate, the fact that the copper interconnect and solder bond had deformed plastically makes it doubtful if linear superposition can be used. In fact, it was mentioned in their paper that their procedure is limited by the solder and copper interconnect plastically deforming that creates a path-dependent result based on the loading history.

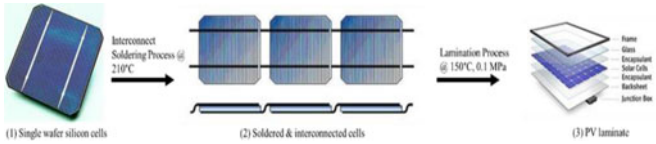

Fig. 2. Typical manufacturing cycle of a conventional wafer-based PV laminate. [5].

In order to properly obtain the accumulated stresses in a PV laminate, each step of the laminate manufacturing cycle should be simulated in a sequential manner whereby the residual stresses developed at the end of one step is brought forward to the next step. Tippabhotla *et al*. [5] performed numerical simulations where the postsoldering stresses were appropriately integrated with the subsequent lamination stresses and postlamination cooldown stresses in a sequential procedure. They found that high stresses arose because of localized bending of the cells during the lamination process. They also measured the stress distribution in the cells using synchrotron X-ray submicron diffraction and found good agreement between measured and simulated stress values. However, they have only considered a single-cell module with a cell design based on a back-contact monocrystalline silicon cell from SunPower, which is a nonconventional interconnect design and not so prevalent.

In this paper, the evolution of stresses in solar cells during the entire manufacturing cycle of a conventional three-busbar, wafer-based PV laminate will be simulated in a sequential manner following the various processes of the manufacturing cycle comprising soldering of interconnect ribbons onto wafer cells, lamination, and postlamination cool down. Furthermore, a multicell laminate, not just one cell as was done in [5], is simulated to investigate any variation in stresses experienced by cells at different locations in the laminate. By analyzing the maximum stresses generated in the cells as they undergo the entire manufacturing cycle, we can identify which are the critical instances in the manufacturing cycle when the stresses in the cells are the largest. We can then assess if these stresses will cause inherent microcracks in the cells to propagate and if so, to what extent, and whether fracture will occur immediately during fabrication or later through temperature cycling and mechanical loading during service.

II. Evolution of Stress in a Photovoltaic Laminate During Its Manufacture

A typical manufacturing cycle of a conventional silicon wafer based PV laminate is illustrated in Fig. 2.

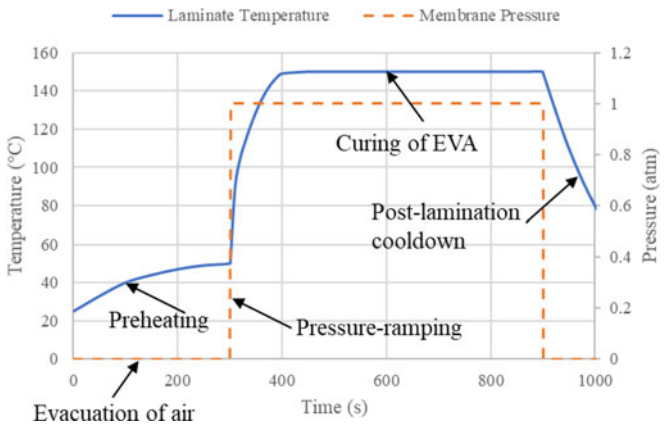

Fig. 3. Variation of pressure differential and temperature in a laminator during the lamination process.

The evolution of stress in the cells during the various processes constituting a typical manufacturing cycle for a conventional silicon wafer based PV laminate is as follows.

A. Interconnect Soldering Onto Cells

Copper interconnects are soldered onto Si wafer cells at temperatures slightly higher than the melting point of the solder used, which is typically 210 °C. At the bonding temperature of 210 °C, it may be assumed that the stress in the assembly is zero. However, when the assembly of cells and interconnects is cooled down to 25 °C, thermal stresses are induced because of the difference in the CTE between the silicon cell and copper interconnects. The maximum stress in the cell during this process will occur at the end of the cool down to 25 °C.

B. Lamination

In this process, a stack-up of glass sheet (bottom most), EVA sheet, interconnected solar cells, EVA sheet, and backsheet are laminated together in a laminator that has upper and lower chambers. At the start of the lamination process, the stack-up is placed onto the laminator table in the lower chamber, which is maintained at a temperature of about 150 °C. However, it has been found that this can cause bowing of the glass sheet, which results in loss of contact at the corners of the glass sheet and, hence, significantly less curing of the EVA near the corners of the laminate. To overcome this problem, a modified procedure has been suggested [15] where lifting pins are used to prop up the stack-up above the laminator table in order to achieve more uniform preheating. In this paper, we will focus on this modified procedure for which the variation of pressure and temperature in the laminator during the lamination process using EVA encapsulant is shown in Fig. 3 [15]. The lamination process can be broken down into three stages, which are described as follows.

1) Evacuation and Preheating: During this stage, both the upper and lower chambers of the laminator are evacuated and the stack-up is preheated to 50 °C. In this stage, there will be some relieving of the postsoldering stress because of the increase in temperature from 25 to 50 °C, which means that the stress here will be lower than that of postsoldering.

2) Pressure Ramping: The lifting pins are now retracted and the upper chamber is vented quickly, which allows the membrane of the upper chamber to press the stack-up onto the heating table. This results in a pressure equivalent to the atmospheric pressure (0.1 MPa), being exerted onto the upper surface of the backsheet. As the EVA is still solid at 50 °C, the pressure load is mechanically transmitted throughout the entire stack-up. In this pressure-ramping step, it is anticipated that the stresses in the cells could be increased because of the additional pressure load.

3) Curing of Ethylene Vinyl Acetate: Upon contact with the laminator table, the temperature of the stack-up rapidly rises to the EVA curing temperature of 150 °C and is maintained at that temperature for some time in order to cure the EVA sufficiently. When the EVA is heated to 150 °C, it melts and flows around the cells and interconnects under the action of the laminator membrane pressure. The load that is now experienced by the interconnected cell array is a hydrostatic pressure of 0.1 MPa as the EVA is now molten. In addition to this, because of the temperature increase to 150 °C, there is substantial further relief of the postsoldering stress. As the hydrostatic pressure on the cells and the stress relief because of the higher temperature both lead to lower the maximum principal stress in the cell, the stress in the cells at the end of this curing stage should be less than the postsoldering stress.

C. Postlamination Cooldown

After the lamination process, the vacuum in the lower chamber is released and allowed the laminate to cool down from 150 to 25 °C. Again, because of the differences in the CTEs of the different constituent materials in the laminate, thermal stresses will arise, which will cause significant changes in the distribution of stresses in the cells. As the temperature change during this cooldown process is large, the stress in the cells could be large at the end of the cooldown process.

In Section III, the evolution of stress in the laminate, in particular, the cells, throughout the entire manufacturing cycle will be simulated using the FE method. From this, the critical instance in the entire manufacturing cycle when the stress in the cells is the highest will be determined. As we are studying the cracking of silicon solar cells and since silicon is a brittle material, the maximum principal stress in the cells will be analyzed.

III. Finite Element Modeling and Analysis

Fig. 4 shows the plan view of a typical conventional 66-cell PV laminate. From the EL image of a typical wafer-based PV module in Fig. 1, it can be seen that almost all the cracks are located along the cell adjacent to the edge of the copper interconnects. This suggests that the maximum stresses in the cells are most likely located in these regions. Although the nature of the problem is 3-D, in order to determine the stresses in the cell along the edges of the interconnects, taking into account the geometry of the interconnected cells, it can be seen in Fig. 4 that a 2-D FEA of a typical cross Section A–A (transverse section across a row of cells) should be sufficient. As such, a 2-D plane-strain model across Section A–A should be able to

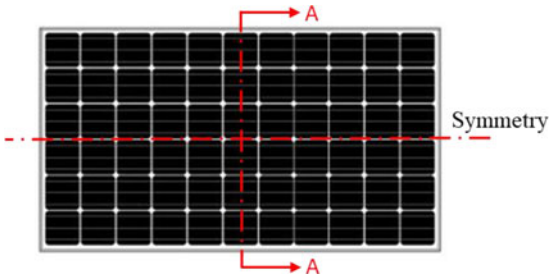

Fig. 4. Plan view of a typical conventional 66-cell silicon-wafer-based PV laminate [picture taken from public domain].

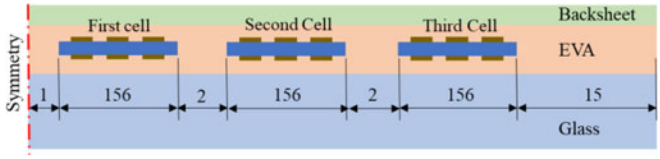

Fig. 5. Cross-sectional view of the PV laminate along A–A. (Not to scale).

TABLE I
MATERIAL PROPERTIES USED FOR THE FEA [7], [13], [16], [17]

Material	E (GPa)	T (°C)	Poisson's ratio	Density (kg/m^3)	CTE $\times$ 10^6 (K^{-1})	T (°C)
					2.61	27
Silicon	130	–	0.28	2329	2.92	67
					3.34	147
Copper (ribbon)	85.7	25				
	82	125	0.3	7329	1.70	–
	79.2	225				
Glass	73	–	0.235	2720	8.00	–
Backsheet	2.075	–	0.3	1370	88.0	–
	0.0153	16				
	0.0096	35				
	0.0079	42				
EVA[a]	0.0019	65	0.4	945	270	–
	0.0012	73				
	0.001	78				
	0.0009	150				

[a]The variation of E of EVA with T was measured by the authors using DMA.

provide a fundamental understanding of the basic physics of stress evolution throughout the manufacturing cycle of a PV laminate. The FE model developed assumes symmetry about the central axis (see Fig. 4) and only one half of the laminate needs to be considered in the simulations.

A schematic of the FE model is shown in Fig. 5. The width of the PV laminate is 976 mm. The cell dimensions are 156 mm $\times$ 156 mm $\times$ 0.18 mm. The thicknesses of the glass, EVA, and backsheet are 3.2, 0.4, and 0.3 mm, respectively.

The PV laminate modeled in this paper consists of glass, copper interconnects on Si-cells encapsulated in EVA, and a polymer backsheet. The material properties used are obtained from the literature and presented in Table I. Solder was not modeled as the thickness of the solder bond is approximately 10 μm and considered too thin to absorb mechanical stresses [6]. The copper interconnect has an elastic–plastic (with isotropic hardening) behavior, whereas temperature-dependent properties are also used for the other materials. The FE model was meshed

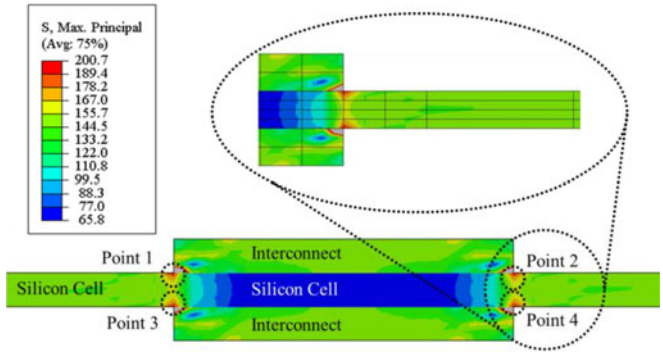

Fig. 6. Maximum principal stresses (MPa) in silicon cell postsoldering.

with eight-node quadratic (CPE8) elements and a mesh refinement study had been carried out that verified that the final mesh used was sufficiently accurate. The effect of gravity was also taken into account.

From the analysis of the evolution of stress in the cells during the various segments of the manufacturing cycle in Section II, the following simulation steps will be performed using Abaqus in a sequential manner. This way, the residual stresses in the cells at the end of one simulation step are sequentially carried forward to the next simulation step.

A. Interconnect-Soldering Step

In this step, only the elements in the interconnects and cells are involved. The common nodes between the interconnects and the cells are tied and a thermal load of −185 °C (25–210 °C) is applied.

B. Preheating Step

In this step, only the elements in the interconnects and cells are involved. A thermal load of +25 °C (50–25 °C) is applied.

C. Pressure-Ramping Step

In this step, the elements of the EVA sheets, backsheet, and glass are added to the cell and interconnect elements. A uniform 0.1 MPa pressure load is applied on the upper surface of the backsheet. A uniform temperature of 50 °C is applied to the entire assembly. The entire bottom surface of the glass sheet is fixed while contact conditions are applied at all contacting surfaces. It should be noted that at 50 °C, the EVA sheets are still solid and can transmit loads mechanically to the cells.

D. Ethylene Vinyl Acetate Curing Step

In this step, the temperature of the assembly is increased from 50 to 150 °C. The EVA melts and fully encapsulates the interconnects and cells. After about 12 min, the EVA is cured (hardened). During this curing period, a uniform pressure of 0.1 MPa on the upper surface of the backsheet is maintained.

E. Postlamination Cooldown Step

In this step, the 0.1 MPa pressure on the upper surface of the backsheet is removed and the laminate cooled down from 150 to

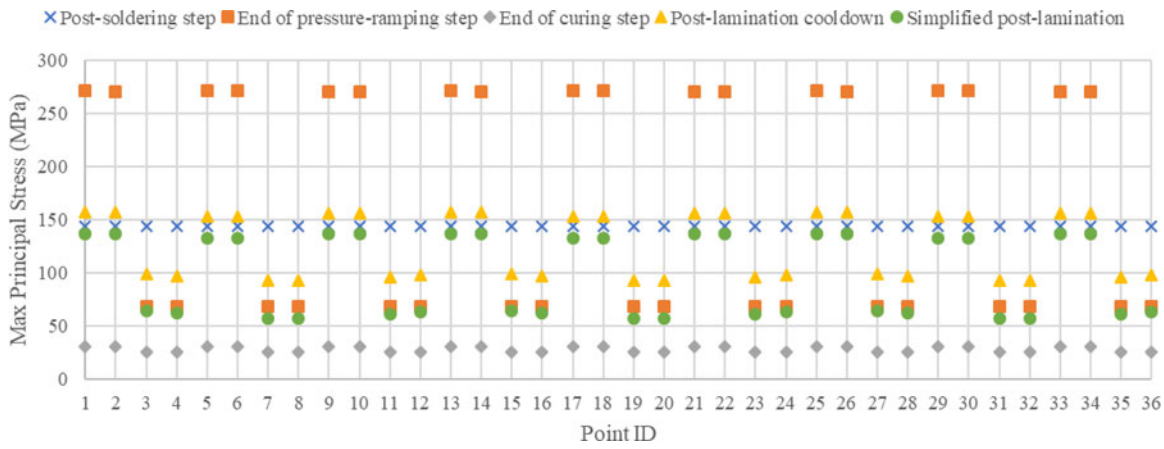

Fig. 7. Plot of maximum principal stress at 36 critical points in three cells throughout the manufacturing process.

25 °C. The bottom leftmost node on the glass sheet is fixed and all the nodes directly above it are constrained to remain in the vertical plane as this is a plane of symmetry at the center of the laminate. A thermal load of −125 °C (25–150 °C) is applied.

IV. Results

A. Stress Evolution Throughout the Manufacturing Cycle

1) Interconnect-Soldering Step: Thermal residual stresses are developed in the cell when it is cooled down from the solder solidification temperature of 210 °C to the room temperature of 25 °C because of the CTE mismatch between the copper interconnect and the silicon cell. Fig. 6 shows the stress distribution in the cell and interconnects around the interconnect–cell bonds nearest to the center of the laminate, at the end of the interconnect-soldering step. Because of symmetry about the horizontal axis of the cell–interconnects assembly, there is no warpage of the assembly. Fig. 6 also shows some details of the FE mesh where the width of the interconnects are discretized into elements of equal length 0.2 mm. As can be seen, the largest stress in the cells occur at the surfaces of the cells adjacent to the corners of the interconnects because of the stress concentration there. The four such critical points for the two interconnects of the first cell nearest the center of the laminate are labeled as 1, 2, 3, and 4 in Fig. 6. There are two such critical points per interconnect and, hence, 36 critical points altogether for the 3 cells in Fig. 5. It is also found that for the subsequent processes in the manufacturing cycle, the largest stresses occur at one or more of these 36 critical points. Hence, the maximum principal stresses at these 36 critical points will be calculated for all the steps simulated in this study and the results plotted in Fig. 7 for comparison.

As can be seen, the largest maximum principal stresses postsoldering are about 145 MPa and are practically equal for all 36 critical points because of symmetry.

Fig. 8 shows the von Mises stress distribution in the copper interconnects postsoldering. As the yield stress of copper is 95.1 MPa, it can be seen that all parts of the copper interconnects are plastically deformed after soldering and cooling down to room temperature. This shows that assumptions of fully elastic copper interconnects will lead to errors and it is important to

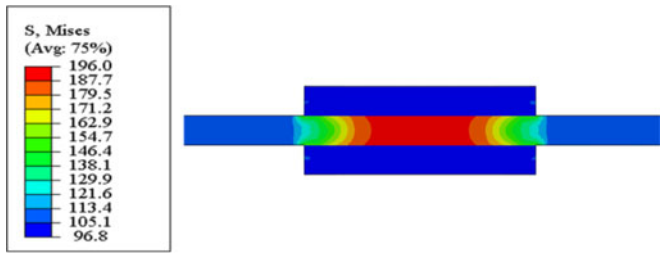

Fig. 8. Von mises stress (MPa) distribution in copper interconnects at 25 °C postsoldering.

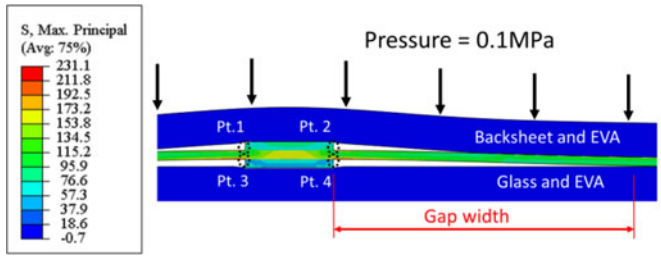

Fig. 9. Stress distribution and cell deformation at the end of the evacuation step. Note the gaps on both sides of the interconnects.

model the copper interconnect material as elastoplastic. A study by Tippabhotla *et al.* [18] has shown that using just linear-elastic properties of copper interconnects overpredicts the stresses in a cell significantly.

2) Pressure-Ramping Step: Fig. 9 shows a close-up view of the region around an interconnect at the end of the pressure-ramping step, which has been obtained by simulation. It is found that on both sides of the interconnects, the EVA sheets are not in contact with the cell and gaps are observed. The largest maximum principal stresses of 275 MPa are found to occur on the backsheet side of the cell as shown in Fig. 7. These values are increased from the 145 MPa tensile postsoldering stress. On the other hand, the maximum principal stresses on the glass side of the cell has decreased to 70 MPa. This can be explained by the fact that the cell which was previously horizontal and flat after soldering is now slightly bent by the pressure load transmitted through the upper solid EVA sheet. The stress distribution in the cell is the superposition of the bending stresses and the

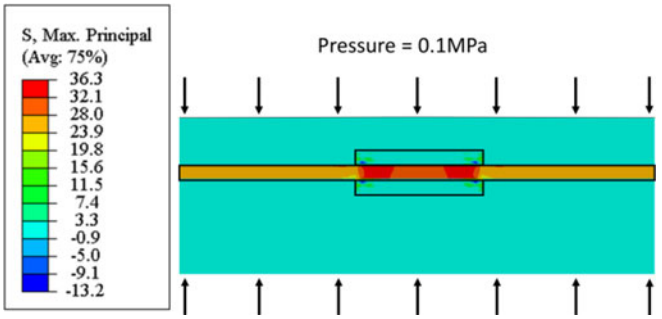

Fig. 10. Cured EVA encapsulating the silicon cell and interconnects with the application of 0.1 MPa at 150 °C (stresses in MPa).

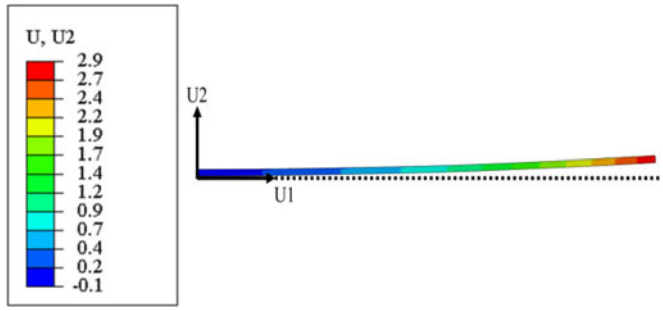

Fig. 11. Warpage of PV laminate at the end of the manufacturing cycle (dimensions in mm).

postsoldering stress distribution. Since bending stresses here are tensile at the top (backsheet side) and compressive at the bottom (glass side) of the cell, the stresses at the critical points on the upper surface of the cell are increased, whereas those at the lower surface of the cell are decreased.

3) Curing Step: In this step, the temperature of the assembly has reached 150 °C and the EVA sheets have melted and flowed to fill up the gaps around the interconnects as can be seen in Fig. 10. The pressure applied on the cells is now a hydrostatic pressure of 0.1 MPa in all directions as the EVA is molten. From Fig. 7, it is observed that the maximum principal stresses have greatly reduced to 20 MPa.

This can be explained by the fact that when the temperature of the assembly reached 150 °C and the EVA becomes molten, the thermal stress at the critical points in the cell are drastically reduced because of the reduced temperature difference of 60 °C (210–150 °C) compared with a temperature difference of 185 °C (210–25°C) after cool down from soldering. Furthermore, the stress arising from the bending of the cell because of the 0.1 MPa pressure from the upper EVA sheet no longer exists as the EVA is now molten and can only exert a hydrostatic pressure on both the upper and lower surfaces of the cell. Being molten, it also offers very little resistance to the restraightening of the cell–interconnect assembly. This is evidenced by the fact that all the stress values for the 36 critical points become approximately equal again, as can be seen in Fig. 7. Thus, at the end of this step, the stresses in the cells are mainly because of the superposition of the thermal stresses because of CTE mismatch between the interconnect and cell for a temperature difference of 60 °C and the hydrostatic pressure. It can be noted that the magnitude of the hydrostatic pressure (0.1 MPa) is negligible in comparison to the thermal stresses.

4) Postlamination Cooldown Step: At the end of the curing step, the vacuum pressure is released and allowed the laminate to cool down from 150 °C to a room temperature of 25 °C. The maximum principal stresses on the backsheet side of the cell are found to be 156 MPa (see Fig. 7), which is marginally higher than the stresses experienced in the postsoldering step. On the glass side of the cell, the principal stresses have values close to 100 MPa.

As mentioned earlier, all numerical simulations of postlamination thermal stress in PV laminates done to date have used what we shall call the simplified postlamination cooldown (SPLC) process [11], [13], where the laminate assembly is assumed to be stress-free at the lamination temperature of 150 °C. Thermal stresses are then developed in the cells on cooling down to room temperature. For comparison purposes, the SPLC was performed for the laminate studied and the results are plotted in Fig. 7 for comparison. It can be observed that the stress values obtained in this paper are 20–30 MPa or 20% higher than that using the SPLC.

Fig. 11 shows the deformed shape of the laminate after postlamination cool down. The laminate (with the glass sheet at the bottom) is observed to warp upwards with an edge deflection of 2.7 mm.

B. Most Critical Instance in Laminate Manufacturing Cycle

The most critical instance in the manufacturing cycle of the PV laminate is the instance when the stress in the cell is the largest. From Fig. 7, it can be clearly seen that the largest stress in the entire manufacturing cycle of a silicon wafer based PV laminate is the instance at the end of the pressure-ramping step. The stress there of 280 MPa is almost double the postsoldering stress of 145 MPa. It is also significantly larger than the stress of 156 MPa after postlamination cool down. Another important point to note is that this level of stress could start growth of the microcracks on the surface of the silicon wafers to larger sizes that subsequently lower the fracture strengths of the silicon cells permanently [19]. While the instance of high stress is not permanent, the damage may already be stored in the materials permanently.

C. Effect of Cell Thickness

The cost of PV modules can be lowered by using thinner silicon cells. However, it is not clear whether thinner silicon cells will or will not lead to larger stresses in the cells. Hence, a further study on the effect of silicon cell thickness on cell stress was carried out. In the simulations carried out earlier, the thickness of the cells was 180 μm. Hence, similar simulations with smaller cell thicknesses of 135 and 90 μm were carried out in this parametric study. Since the stress pattern for the 3 cells is approximately the same (see Fig. 7), only the stresses at the 12 critical points in the first cell are plotted and compared for the different cell thicknesses in Fig. 12.

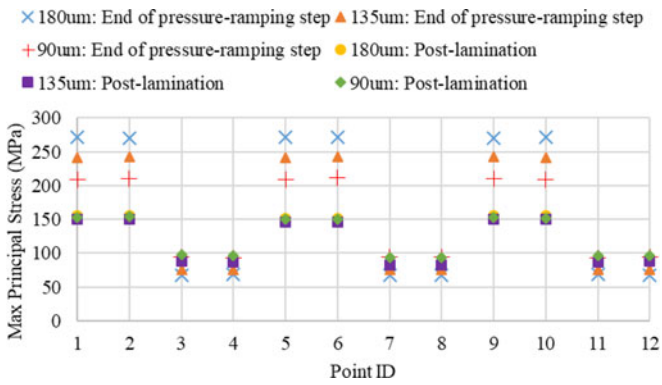

Fig. 12. Plot of maximum principal stresses for cells of different thickness at the end of the evacuation and postlamination cooldown steps.

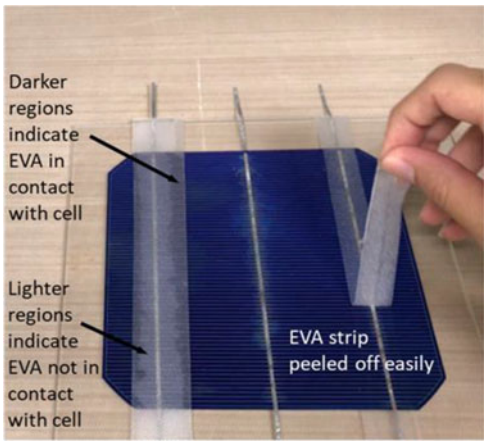

Fig. 13. Experiment verifying assumption of solid EVA during the evacuation step in the lamination process.

From Fig. 12, it can be observed that the maximum principal stresses in the postlamination cooldown step does not change much with cell thickness but that at the end of the pressure step decreases significantly with the decrease in the thickness of the cells, by up to 23% for a decrease from 180 to 90 μm. This trend can be explained in the following manner. Focusing on the critical points 2 and 4 of the cell extending out on the right side of the interconnect, it is known that the stresses at these points are the summation of the postsoldering stress and the bending stress because of the bending of the cells by vacuum pressure after evacuation. The stress at point 2 because of cell bending is in-plane, tensile, and its magnitude given by

$$\sigma_{b2} = \kappa t E/2 \tag{1}$$

where κ is the curvature, E the young's modulus, and t the thickness of the cell. When the thickness t of the cell is decreased, the cell is more compliant resulting in an increase in the curvature κ. This is confirmed from simulation results of gap widths (see Fig. 9) of 8.1, 6.5, and 5.8 mm for t of 180, 135, and 90 μm, respectively. Thus, the thinner the cell the smaller the gap width, which implies that the cell is more compliant. However, from (1), the bending stress is proportional to the product κt which could, thus, increase or decrease with decreasing t. From Fig. 12, it can be seen that the product κt in fact increases with the decrease in t, since the numerical simulation results show that the bending stress σ_{b2} increases with t.

V. Discussion

As the detailed structure, geometry, and dimensions of the cells and the materials used in our PV laminates may be different from those of others, it is difficult to directly compare the stresses obtained in this paper with those of others. Nevertheless, we note that the values of postsoldering maximum principal stresses in the cells obtained by Dietrich *et al.* [14] were 140–150 MPa, and by Rendler *et al.* [20] were 98–205 MPa, which are in good agreement with the value of 145 MPa obtained from our simulations.

It is interesting to note from Fig. 7 that the stress pattern within each cell is approximately the same for all the cells in the transverse cross section of the PV laminate. This is probably true for the stresses at the postsoldering and pressure-ramping steps. However, for the postlamination cooldown step, differences may potentially arise because of the different distances of the cells from the central of the laminate. The fact that the same stress pattern is obtained for all the cells is probably because of the fact that we have presently performed only a 2-D analysis that allowed the laminate to warp in a cylindrical fashion as can be seen in Fig. 11. The situation may be different in a 3-D analysis, which will be attempted next. Nevertheless, as far as the stresses in the evacuation step is concerned, the present 2-D analysis is valid.

One of the basic assumptions in our simulations is that the EVA sheets are still solid during the evacuation and onset of pressure step, and hence, capable of transmitting pressure to the cells. To verify this, an experiment was carried out whereby strips of EVA were placed over the soldered interconnect ribbons of a solar cell (see Fig. 12) with the laminator temperature maintained at 50–60 °C and the evacuation process was executed for 10 min, double the 5 min assumed in this paper. After the 10 min, the cell was taken out of the laminator. It was observed (see Fig. 13) that the EVA had not melted, and on both sides of the interconnect ribbons, there were pockets where the EVA sheets did not touch the cell surface at all. Furthermore, for the adhered portions, it was quite easy to peel off the EVA strips from the cell. This experiment clearly verifies our assumption that the EVA sheets are solid during the evacuation step and our prediction from our simulations that the EVA sheets did not touch the cell along sections on both sides of the interconnect.

It has been shown in this study that although the use of lifting pins in the modified lamination procedure may lead to more uniform curing of EVA across the whole laminate, it has led to the *highest cell stresses* developed in the entire manufacturing cycle at the end of the pressure-ramping step, which makes it the *most critical instance* in the manufacturing cycle. This is because the EVA is still solid at 50 °C and able to transmit the mechanical pressure load onto the cells giving rise to additional localized bending stresses in the cells. It is likely that if the EVA had been preheated to a higher temperature and hence become softer or even liquid, the additional stresses because of the pressure-ramping load may be reduced. Thus, the modified

lamination procedure analyzed in this study may be regarded as a worst-case scenario. However, even without lifting pins, it is possible that because of nonuniform preheating some regions of the EVA sheets may still be solid and give rise to higher cell stresses during pressure ramping.

VI. Conclusion

In this study, the evolution of stresses in the solar cells throughout the entire manufacturing cycle has been analyzed for a modified lamination procedure employing lifting pins. Following this analysis, the largest maximum principal stress in the solar cells of a typical conventional silicon wafer based PV laminate has been determined using FEA of every significant segment of its manufacturing cycle. The final accumulated residual stresses in a conventional, three-busbar, wafer-based PV laminate have been determined that includes the postsoldering, lamination, and postlamination thermal stress. This stress has been found to be about 20% higher than that obtained using the SPLC process done by other researchers to date. In this study, it was found that the stresses in the cells during the pressure-ramping step of the lamination process is the highest in the modified PV laminate manufacturing cycle. As such, there is a tradeoff between uniform curing of EVA and higher stresses developed in cells when using lifting pins during the lamination step. More studies would need to be carried out on lamination recipes to improve the service reliability and throughput of PV laminates. The effects of cell thickness on the evolution of stresses during lamination were also investigated and it was found that thinner cells led to lower cell stresses.

References

[1] M. Köntges, I. Kunze, S. Kajari-Schröder, X. Breitenmoser, and B. Bjørneklett, "The risk of power loss in crystalline silicon based photovoltaic modules due to micro-cracks," *Sol. Energy Mater. Sol. Cells*, vol. 95, no. 4, pp. 1131–1137, 2011.

[2] "Imaging of Solar Cells and Modules," *Sensovation.com*, 2017. [Online]. Available: http://www.sensovation.com/bausteine.net/i/36089/HR-830CZ25mmModule.jpg?width=560. Accessed on: Mar. 1, 2017.

[3] S. Kajari-Schröder, I. Kunze, U. Eitner, and M. Köntges, "Spatial and orientational distribution of cracks in crystalline photovoltaic modules generated by mechanical load tests," *Sol. Energy Mater. Sol. Cells*, vol. 95, no. 11, pp. 3054–3059, 2011.

[4] M. Sander *et al.*, "Characterization of PV modules by combining results of mechanical and electrical analysis methods," in *Proc. Eur. Photovolt. Sol. Energy Conf. Exhib.*, Valencia, Spain, 2010, pp. 3993–3997.

[5] S. Tippabhotla *et al.*, "From cells to laminate: Probing and modeling residual stress evolution in thin silicon photovoltaic modules using synchrotron X-ray micro-diffraction experiments and finite element simulations," *Prog. Photovolt. Res. Appl.*, vol. 25, no. 9, pp. 791–809, 2017.

[6] F. Kraemer, J. Seib, E. Peter, and S. Wiese, "Mechanical stress analysis in photovoltaic cells during the string-ribbon interconnection process," in *Proc. 2014 15th Int. Conf. Thermal, Mech. Mulit-Phys. Simul. Exp. Microelectron. Microsyst.*, 2014, pp. 1–7.

[7] S. Dietrich, M. Pander, M. Sander, S. Schulze, and M. Ebert, "Mechanical and thermomechanical assessment of encapsulated solar cells by finite-element-simulation," in *Proc. Rel. Photovolt. Cells, Modules, Compon., Syst. III*, 2010, vol. 7773, Paper 77730F.

[8] U. Eitner, M. Pander, S. Kajari-Schröder, M. Köntges, and H. Altenbach, "Thermomechanics of PV modules including the viscoelasticity of EVA," in *Proc. 26th Eur. Photovolt. Sol. Energy Conf. Exhib.*, Hamburg, Germany, 2011, pp. 3267–3269.

[9] U. Eitner, S. Kajari-Schröder, M. Köntges, and R. Brendel, "Non-linear mechanical properties of ethylene-vinyl acetate (EVA) and its relevance to thermomechanics of photovoltaic modules," in *Proc. 25th Eur. Photovolt. Sol. Energy Conf. Exhib.*, Valencia, Spain, 2010, pp. 4366–4368.

[10] U. Eitner, M. Köntges, and R. Brendel, "Use of digital image correlation technique to determine thermomechanical deformations in photovoltaic laminates: Measurements and accuracy," *Sol. Energy Mater. Sol. Cells*, vol. 94, no. 8, pp. 1346–1351, 2010.

[11] Y. Lee and A. A. O Tay, "Finite element thermal stress analysis of a solar photovoltaic module," in *Proc. 2011 37th IEEE Photovolt. Spec. Conf.*, 2011, pp. 003179–003184.

[12] Y. Lee and A. A. O Tay, "Stress analysis of silicon wafer based photovoltaic modules in operation," in *Proc. 2012 38th IEEE Photovolt. Spec. Conf.*, 2012, pp. 003172–003177.

[13] Q. Zhang *et al.*, "Numerical investigation on residual stress in photovoltaic laminates after lamination," *J. Mech. Sci. Technol.*, vol. 29, no. 2, pp. 655–662, 2015.

[14] S. Dietrich, M. Pander, M. Sander, U. Zeller, and M. Ebert, "Stress analysis of encapsulated solar cells by means of superposition of thermal and mechanical stresses," in *Proc. SPIE*, 24 Sep. 2013, vol. 8825, Paper 882505.

[15] H. Li, L. Perret-Aebi, V. Chapuis, C. Ballif, and Y. Luo, "The effect of cooling press on the encapsulation properties of crystalline photovoltaic modules: Residual stress and adhesion," *Prog. Photovolt. Res. Appl.*, vol. 23, no. 2, pp. 160–169, 2013.

[16] U. Eitner, "Thermomechanical analysis of photovoltaic modules," Ph.D. dissertation, Centre Eng. Sci., Martin Luther Univ. Halle-Wittenberg, Halle, Germany, 2011.

[17] O. Hasan, A. Arif, and M. Siddiqui, "Finite element modeling, analysis, and life prediction of photovoltaic modules," *J. Sol. Energy Eng.*, vol. 136, no. 2, 2013, Art. no. 021022.

[18] S. Tippabhotla *et al.*, "Effect of interconnect plasticity on soldering induced residual stress in thin crystalline silicon solar cells," in *Proc. 2016 IEEE 18th Electron. Packag. Technol. Conf.*, 2016, pp. 734–737.

[19] M. Demant *et al.*, "Microcracks in silicon wafers and solar cells: Detection and rating of mechanical strength and electrical quality," in *Proc. 29th Sol. Energy Conf. Exhib.*, 2014, pp. 390–396.

[20] L. C. Rendler, A. Kraft, C. Ebert, S. Wiese, and U. Eitner, "Investigation of thermomechanical stress in solar cells with multi busbar interconnection by finite element modeling," in *Proc. 32nd Eur. Photovolt. Sol. Energy Conf.*, 2015, pp. 94–98.

Authors' photographs and biographies not available at the time of publication.